STUDY OF THE TRANSVERSE BED TOPOGRAPHY AT BENDS OF THE ALLUVIAL RIVERS

Kassem Salah Abdel Wahab El-Alfy

Associate Prof., Irrigation and Hydraulics Dept., Faculty of Engineering,
Mansoura University, Egypt

ABSTRACT

In this paper, a mathematical model for studying the lateral bed topography of the alluvial rivers at bends is presented. The effect of the suspended sediment is excluded from this model. The field measuring of the cross-sections is carried out on twenty-one bend positions on Damietta Nile branch downstream Zefta barrages, in Egypt. A comparative study is carried out between both the measured lateral bed topography and that resulted from application of the mathematical model at the different bends under study. It is found that there is a difference of about 5%-31% between the measured values of the dimensionless flow depth (H/H^-) and the corresponding computed ones at the different values of the dimensionless radius of the bend (R/R^-) up to the zone of the maximum flow depth. The study shows that beside the effect of the radius of curvature on the lateral bed topography at the bends, the hydraulic radius of the stream at bends has also a considerable effect. Also, the lateral diffusion of the suspended sediment has negligible effect on the lateral bed topography of the cross-section in Damietta Nile branch, in Egypt. It is found that the angle of slope of the outer bank at the bend is inversely proportional to the bend radius, while the angle of slope of the inner bank is directly proportional to the bend radius. Finally, it can be concluded that the lateral bed topography in non-uniformly curved bends in Damietta Nile branch, in Egypt can be predicted based on the mathematical model presented in this paper by an error ranges between 5%-31% up to the zone of the maximum flow depth (R/R^-=1-1.18).

1. INTRODUCTION

The meandering river consists of a series of deep pools in the bends and shallow crossings in the short straight reach connecting these bends. The meandering phenomenon has engendered great interest as evidence by the number of papers on the subject to be found in the literature. In 1957 Lane [10] concluded that a meandering stream is one whose channel alignment consists principally of pronounced bends. In general, the bends are formed by the process of erosion and deposition. At bends, a considerable amount of eroded material from the outer bank is normally deposited over a period of time on the inner bank, while the rest is deposited on the point bars that are formed in the downstream. Under these conditions, the channel would simply widen until it becomes so large that the erosion would terminate. As a meandering river system moves laterally and longitudinally, the meander loops move at an unequal rate because of the unequal erodibility of the banks. This causes a tip or bulb to form

and ultimately this tip or bulb is cut off. After the cut off has formed a new bend may slowly developed. Its geometry depends upon the local slope, the bank material, and the geometry of the adjacent bends. Years may be required before a configuration characteristic of the average conditions in the river is attained.

Van Bendegom [17], Yen [18], Kikkawa et al. [9], Zimmermann and Kennedy [19], Falcon [6], and Odgaard [13] introduced notable contributions to the advances in theory and practical application of the bed topography in bends. Their studies were based on the lateral force balance between the fluid force exerting on bed material and the gravity force. Parker [14] treated analytically the lateral bed topography of self-formed straight channels of a noncohesive soil. He [14] concluded that the lateral channel geometry bases on the bed load that moves down the lateral slope of the bank to the channel center due to the fluid force and gravity. In 1957, Rozovskii [15] described a uniformly curved reach of the Desna River, a branch of Dniepr in USSR. Also, Jackson [7,8] studied several curved reaches of the lower Wabash River, Illinois and Indiana, in which the bed material is actively transported as suspended load. In 1999 Blanckaert et al. [2] studied the flow in open channel bends experimentally. In 2000 Nagata et al. [12] studied the aforementioned phenomena by using the numerical analysis. In 2001 Blanckaert et al. [3,4] studied the turbulence occurs in open channel at bends. Thus, the mechanism for defining the lateral bed profile in curved alluvial channels still requires more studies.

2. THE MATHEMATICAL MODEL

The concentration of the suspended sediment in unidirectional flow decreases monotonously, approaching the free surface and the distribution is approximately typically with exponential curve [1]. As stated by Parker [14], in wide-open channel the lateral transport of the suspended sediment load is occurred by the secondary flow and the turbulent diffusion. In wide open channel, the component of the secondary flow is directed towards the outer bank in the upper flow layer, while it is directed towards the inner curve for the lower layer. Then at the equilibrium condition;

$$Q_{CL} + Q_{DL} + Q_{BL} = 0 \qquad (1)$$

in which

Q_{CL} vertically integrated lateral volumetric transport of suspended sediment per longitudinal unit length due to secondary flow.

Q_{DL} vertically integrated lateral volumetric transport of suspended sediment per longitudinal unit length due to turbulent diffusion.

Q_{BL} lateral volumetric bed load transport rate per longitudinal unit length.

When Q_{CL} and Q_{DL} equal zero for nonsuspendable bed load material, the equilibrium is achieved when

$$Q_{BL} = 0. \qquad (2)$$

As stated by Kikkawa et al. [9], the velocity distribution of the secondary flow at bends in open channel can be written in the following form:

$$\frac{U_r}{U^-} = f^2 \frac{H}{R}\frac{1}{k}\left[F_1(\eta) - \frac{1}{k}\frac{U_*^-}{U^-}F_2(\eta)\right] = f^2 \frac{H}{R}\frac{1}{k}F(\eta) \quad (3)$$

in which:

U_r the lateral velocity component of the secondary flow,
$F(\eta)$ function of η and $\eta = 1 + Z/H$

$$F_1(\eta) = -15\,(\eta^2 \ln \eta - 0.5\,\eta^2 + 0.28) \quad (4)$$

$$F_2(\eta) = -7.5\,(\eta^2 \ln^2 \eta - \eta^2 \ln \eta + 0.5\,\eta^2 - 0.352) \quad (5)$$

As stated by Syunsuke et al. [16], $F_1(\eta)$ and $F_2(\eta)$ can be approximated in the following polynomials form:

$$F_1(\eta) = -12.056\,\eta^3 + 14.997\,\eta^2 + 4.6096\,\eta - 4.2898 \quad (6)$$

$$F_2(\eta) = -5.31\eta^2 + 9.143\,\eta - 2.802 \quad (7)$$

As stated by Blanckaert et al. [2], the vertical concentration distribution of the suspended sediment is given by the following equilibrium equation:

$$V_s c + \varepsilon_{sz}\frac{dC}{dZ} = 0 \quad (8)$$

in which

V_s the fall velocity of sediment,
c local concentration of suspended sediment.

Syunsuke et al. [16] stated that the solution of Eq. (8) subjected to the boundary condition at the bed $C = C_0$, which is given by:

$$C = C_0 \exp\left[-\frac{V_s}{\varepsilon_{sz}}(Z + H)\right] \quad (9)$$

in which

$$C_0 = 2.31 * 10^{-4}\left(\frac{U_*}{V_s}\right) \quad \text{for } U_*/V_s \le 88.3 \quad (10)$$

ε_{sz} is the vertical eddy diffusivity of suspended sediment = $0.077 U_* H$

The vertically integrated lateral volumetric flux of the suspended sediment due to secondary flow can be given by

$$Q_{CL} = \int_{-H}^{0} U_r c\, dZ \quad (11)$$

Syunsuke et al. [16] stated that the following relationship can be used in computing the lateral convective transport of the suspended load:

$$\frac{Q_{CL}}{U^- H} = -f^2 \frac{H}{R}\Phi_{CL} \quad (12)$$

in which Φ_{cL} is a dimensionless function [16].

The lateral volumetric flux of the suspended sediment due to turbulent diffusion can be computed as [14]:

$$Q_{DL} = -\varepsilon_{sr} \frac{dC}{dR} \tag{13}$$

$$C = \int_{-H}^{0} c dZ \tag{14}$$

in which:

ε_{sr} the lateral eddy diffusivity = $0.13U_*H$ [16], and

C the vertically-integrated concentration

Substitution of Eq. (9) and Eq. (10) into Eqs. (13) and (14) yields

$$\frac{Q_{DL}}{U_* H} = -\frac{dH}{dR} \Phi_{DL} \tag{15}$$

in which Φ_{DL} is a dimensionless function [16]

The movement of the bed load in river bends was treated analytically by Kikkawa et al. [9]. Parker [14] reduced Kikkawa et al. [9] results to the following form:

$$\frac{Q_{BL}}{Q_B} = \tan\delta + \frac{1+\alpha\mu}{\lambda\mu} \sqrt{\frac{\tau_{*c}}{\tau_*}} \tan\theta \tag{16}$$

in which:

Q_{BL} lateral volumetric bed load per unit length.

Q_B longitudinal volumetric bed load per unit length.

μ dynamic coefficient of Coulomb friction = 0.43.

α ratio of lift coefficient to drag coefficient.

Λ sheltering coefficient = 0.59.

τ_* dimensionless shear stress = $U_*^2/R_s gd$.

R_s submerged specific gravity of sediment = 1.65 for natural bed material.

τ_{*c} dimensionless critical shear stress = 0.06.

θ lateral slope of bed.

δ angle between the near bed flow velocity and longitudinal direction, which can be determined according to [9] as follows:

$$\tan\delta = \frac{U^-}{U_*^-} \frac{F(0)}{A_r} \frac{H}{R} \tag{17}$$

in which:

A_r (constant) = 8.5 : [1]

$F(0) = -4.167 + 2.64U_*^- / kU^-$ [1]

Substitution of Eq. (17) into Eq. (16) yields

$$\frac{Q_{BL}}{Q_B} = f\frac{H}{R}(1.941-1.226\frac{U^-}{U_*^-})+5.382\sqrt{\frac{\tau_{*c}}{\tau_*}}\frac{dH}{dR} \tag{18}$$

in which

α constant =0.85 : [9]; and

dH/dR = tanθ

Einstein [5] derived the following simple equation to compute the longitudinal volumetric bed load per unit length as:

$$Q_B = 11.2\sqrt{R_s g d^3}\frac{(\tau_* - 0.03)}{\tau_*^3} \tag{19}$$

in which d is mean diameter of the bed material

Syunsuke [16] stated the following basic equation to define the lateral bed profile in uniformly-curved channels:

$$\frac{dH}{dR} = f\frac{H}{R}\frac{Q_B\left(-1.941+1.226\frac{U^-}{U_*^-}\right)+fUH\Phi_{CL}}{5.382Q_B\sqrt{\frac{\tau_{**c}}{\tau_*}}-U_*H\Phi_{DL}} \tag{20}$$

Eq. (20) can be rewritten in the following form

$$\frac{dh}{dr} = f\frac{h}{r}\frac{q_B\left(-1.941+1.226\frac{U^-}{U_*^-}\right)+f\frac{H^-}{d}\frac{U^-}{U_*^-}\sqrt{\tau_*}\Phi_{CL}h}{5.382\frac{q_B}{f}\sqrt{\frac{\tau_{**c}}{\tau_*}}-f\frac{H^-}{d}\sqrt{\tau_*}\Phi_{DL}h} \tag{21}$$

in which

h the dimensionless depth = H/H$^-$

r the dimensionless lateral distance = R/R$^-$

q the dimensionless longitudinal bed load = $Q_B/\sqrt{R_s g d^3}$.

f_*=f the dimensionless shear velocity =U_*/U_*^- .

q_B is correlated with $\tau_B = f^2\tau_*^-$.

Φ_{DL} *and* Φ_{CL} are functions of $U_*/V_s = fU_*^-/V_s$.

From Eq. (21), it can be concluded that the lateral bed profile is controlled by the dimensionless parameters τ_*^-, H_*^- / d, U^- / U_*^-, U_*^- / V_s and f. V_s is the sediment fall velocity depends on d_{50} of the particles. $\tau_* = U_*^2 / R_s gd$ and U_*/V_s are not independent parameters, then the independent variables parameters are therefore reduced to τ_*^-, U^- / U_*^- and R^- / B.

Depending on these dependent and independent variables Eq. (21) can be numerically integrated with the boundary condition h=1 at r =1. Assuming small suspended load (i.e. $\Phi_{DL} = \Phi_{CL} = 0$ [16]), then Eq. (21) can be reduced to:

$$\frac{dh}{dr} = f^2 \frac{h}{r} \frac{-1.941 + 1.226 \dfrac{U^-}{U_*^-}}{5.382 \sqrt{\dfrac{\tau_{**c}}{\tau_*}}} \qquad (22)$$

Kikkawa et al. [9] made a comparison between the results of Yen study [18] and the corresponding values resulted by Eq. (22). Kikkawa et al. [9] concluded that Eq. (22) gave good agreement with Yen [18] study. Also, Eq. (22) was rested by Odgaard study [13] and he found that there was good agreement between the measured and the predicted values by Eq. (22) if calibration factors of 0.76 and 2.0 were imposed on Eq. (22) for the laboratory and field measurements, respectively. Mori and Kishi [11] applied Eq. (22) on a bend of Ishikari River in Japan which was reversed that Eq. (22) requires a calibration factor of 0.35.

3. FIELD MEASUREMENTS

The field measurements are carried out on Damietta Nile branch downstream Zefta barrages at many bend locations in cooperation with the Hydraulic Research Institute (HRI), National Water Research Center, Ministry of Water Resources and Irrigation, Egypt. At each bend location, the inner radius of the bend, the outer radius of the bend, the bed width and the radius at the centerline of the bend were measured. Also, the profile of the cross-section at each bend location was measured. From the profile of the cross-section at each bend site, both the water depth and the mean flow velocity at the centerline were calculated. Also, the maximum values of the scour depth at the outer bank at the different bend positions were measured. The slope of the lateral bed profile in directions of both the inner and the outer banks were also measured. Also, the cross-sectional area, the wetted perimeter, the discharge were measured at different cross-sections. A bed sample at each bend position was taken and the grain size distribution curve was drawn to determine the median grain size of the bed particles, d_{50}. The median diameter of the bed ranged between 0.22 mm to 0.268 mm. Also, the discharge ranged between 30 to 25 million cubic meters per day. The different properties of the different bend locations are illustrated in Table (1), Appendix.

4. ANALYSIS AND DISCUSSION OF THE RESULTS

The relationships between the dimensionless geometrical radius (R/R^-) and the corresponding dimensionless maximum flow depth at the outer-bank (H/H^-) at different points at fourteen selected bends cross-sections of the bends under study on Damietta Nile branch are shown through Figs. (1) to (14) for both the measured and the computed values of the lateral bed topography. Fig. (1) illustrates the relationship between H/H^- and $R/\acute{R}$ at km 91.550 on Damietta Nile branch. The figure shows that the difference between both the measured and the computed values of H/H^- at each value of $R/\acute{R}$ ranges between 18%-31% up to the zone of the maximum depth (at $R/\acute{R}$=1.03). Fig. (2) illustrates the relationship between H/H^- and $R/\acute{R}$ at km 92.250 on Damietta Nile branch. It was found that the dimensionless computed maximum flow depth equals to 133% of the measured one at the dimensionless radius equals to 1.10. This can be explained due to the fact that the computed values of H/H^- was inversely proportional to the bend radius, while the measured values of H/H^- depended on the lateral connective force, which depended upon the bend radius besides the flow velocity.

Figs. (3, 4, 5, 8), and Fig. (9) showed that the difference between both the measured and the calculated values of the dimensionless flow depth at the value of zone of the maximum flow depth ($R/\acute{R}$ =1.0-1.18) ranged from 5% to 17%. Fig. (10) showed that the maximum computed value of H/H^- at R/R^- =1.045 was about 12%, which is less than the corresponding measured value. Figures (12) and (14) showed that the computed values of H/H^- at the different values of R/R^- was smaller than the corresponding measured by about 25% up to the point of the maximum flow depth.

Fig. (15) shows the relationship between both the outer bank and the inner bank slope angles and the bend radius at different bends under study on Damietta Nile branch. The figure showed that the angle of slope of the outer bank was inversely proportional to the bend radius, while the angle of slope of the inner bank was directly proportional to the bend radius. This could be attributed due to the fact that the decrease of the bend radius increased the scour at the outer bank of the cross-section i.e. the depth of the cross-section increase, which increased the slope of the side slope provided that the cross-section was cohesive soil as it was found in this research paper. The increase of the scour at the outer bank of the bend was accompanied with a deposition in the inner bank, which decreased the angle of the slope of the inner bank of the bend. Fig. (16) shows the relationship between the dimensionless maximum scour depth at the outer bank and the hydraulic radius. The figure showed that the maximum dimensionless scour depth at the outer bank was directly proportional to the hydraulic radius. This could be explained due to the increase of the flow velocity due to the increase of the hydraulic radius, which increased the centrifugal force of the flowing water on the outer bank.

From the analysis of the results, it could be concluded that the difference occurred between the measured values of H/H^- at different values of R/R^- and the

corresponding computed ones was referred to the fact that the effect of the suspended load was excluded from the mathematical model. Also, it was found that the difference between the measured values and the computed values at the outer bank of the bend could be referred to the effect of the considerable lateral connective transport produced by the effect of the centrifugal force at the outer region of the bend. The study illustrated that the mathematical model can be used to predict the lateral bed profile in uniformly-curved bends in Damietta Nile branch by using a correction factor equals to 5-31% up to the zone of the maximum flow depth (R/R^-=1-1.18).

5. CONCLUSIONS

It can be concluded that the lateral bed topography in uniformly-curved bends in Damietta Nile branch, in Egypt can be predicted based on the mathematical model presented in this paper by using a correction factor equals to 5-31% up to the zone of the maximum flow depth (R/R^-=1-1.18). Also, it can be concluded that the hydraulic radius of the cross-section has a considerable effect beside the effect of the radius of curvature on the lateral bed topography. The difference between the measured values of H/H^- at different values of R/R^- and the corresponding computed ones can be referred to the fact that the effects of the suspended load are excluded from the mathematical model. Also, it can be concluded that the lateral diffusion of the suspended sediment has negligible effect on the profile of the cross-section. It is found that the angle of the outer bank of the bend site is inversely proportional to the bend radius, while the angle of the inner bank of the bend is directly proportional to the bend radius. Also, the maximum dimensionless scour depth at the outer bank is directly proportional to the hydraulic radius of the cross-section.

ACKNOWLEDGEMENTS

The field measurements in this research paper were carried out in cooperation with the Hydraulic Research Institute (HRI), National Water Research Center, Ministry of Water Resources and Irrigation. The different instruments, apparatuses, and the financial supports were provided by Hydraulic Research Institute (HRI), National Water Research Center, Ministry of Water Resources and Irrigation. This is gratefully acknowledged.

NOMENCLATURE

The following symbols are used in this research paper:

B channel width;
c local concentration of suspended sediment;
d bed material size;
h the dimensionless depth = H/H^-;
r the dimensionless lateral distance = R/R^-;
H flow depth at the outer bend curvature;
H^- flow depth at the center of the cross-section;

q the dimensionless longitudinal bed load = $Q_B / \sqrt{R_s g d^3}$;
Z vertical distance from free surface of water;
A_r constant = 8.5;
Q_B longitudinal volumetric bed load per unit length;
Q_{BL} lateral volumetric bed load transport rate per longitudinal unit length;
Q_{CL} vertically integrated lateral volumetric transport of suspended sediment per longitudinal unit length due to secondary flow;
Q_{DL} vertically integrated lateral volumetric transport of suspended sediment per longitudinal unit length due to turbulent diffusion;
U_r the lateral velocity component of the secondary flow;
V_s the fall velocity of sediments;
ε_{sz} the vertical eddy diffusivity of suspended sediment = $0.077U_*H$;
Φ_{cL} a dimensionless function;
ε_{sr} the lateral eddy diffusivity =$0.13U_*H$;
Φ_{DL} a dimensionless function;
α ratio of lift coefficient to drag coefficient = 0.85;
λ sheltering coefficient = 0.59;
τ_* dimensionless shear stress = $U_*^2/R_s gd$;
R_s submerged specific gravity of sediment = 1.65 for natural bed material;
τ_{*c} dimensionless critical shear stress = 0.06;
θ lateral slope of bed;
δ angle between the near bed flow velocity and longitudinal direction;
μ dynamic coefficient of Coulomb friction = 0.43; and
f_* the dimensionless shear velocity =$U_*/\bar{U_*}$.

REFERENCES

1- Ashida, K., and Michiue, M., "Study on the suspended sediment", Disaster Prevention Research Institute Annuals, Kyoto University, Kyoto, Japan, No. 13B, pp. 23-242 (in Japanese), 1970.
2- Blanckaert, K., and Graf, W. H., "outer-bank cell of secondary circulation and boundary shear stress in open channel bends", Proc., Symp. on River coastal and Estuarine Morphodynamics, University of Genova, Italy, Vol. 1, pp. 533-543, 1999b.
3- Blanckaert, K., and Graf, W. H., "Experiments on flow in a strongly curved channel bend", Proc., 29th Congr. Int. Assoc. Hydr. Res. and Engrg., Chinese Hydraulic Engineering Society, Beijing, China, 2001.
4- Blanckaert, K., and Walter H. Graf, "Mean flow and turbulence in open-channel bends", Journal of Hydraulic Engrg. ASCE, 127, No. 10, pp. 835-847, October 2001.
5- Einstein, H. A., and Chien, N., "Effect of heavy sediment concentration near the bed on velocity and sediment distribution", Inst. of Eng. Research, Univ. of California, Berkeley, California, USA, 1955.

6- Falcon, M. A., "Analysis of flow in alluvial channel bends", thesis presented to the University of Iowa, at Iowa City, Iowa, in partial fulfillment of the requirements for the degree of Doctor of Philosophy, 1979.
7- Jackson, R. G., "Velocity-bed-form texture pattern of meander bends in the lower Wabash River of Illinois and Indiana", Geological Society of America Bulletin, Vol. 86, pp. 1511-1522, 1975.
8- Jackson, R. G., "Unsteady-flow distribution of hydraulic and sedimentologic parameters across meander bends of the lower Wabash River of Illinois and Indiana", Proceeding of International Symposium on steady flow in open channels, BHRA Fluid Engineering, Granfield, Bedford, England, pp. G4.35-48, 1976.
9- Kikkawa, H., Ikeda, S., and Kitagawa, A., "Flow and bed topography in curved open channels", Journal of Hydraulic Division, ASCE, Vol. 102, No. HY9, pp. 1327-1342, 1976.
10- Lane, E. W., "A study of the shape of channels formed by natural streams flowing in erodible material", Missouri River Division Sediments Series No. 9, U.S. Army Engineering Division, Missouri River, Corps of Engineers, Omaha, Nebraska.
11- Mori, A., and Kishi, T., "A study on bed topography in channel bend", Proc. Of Japanese Conference on Hydraulics, Japan Society of Civil Engineers, No. 26, pp. 63-68, 1982.
12- Nagata, N., Hosoda, T., and Muramoto, Y., "Numerical analysis of river channel processes with bank erosion", Journal of Hydraulic Engrg. ASCE, 126(4), pp. 243-252, 2000.
13- Odgaard, A. J., "Transverse bed slope in alluvial channel bends", Journal of Hydraulic Division, ASCE, Vol. 107, No. HY12, pp. 1677-1694, 1981.
14- Parker, G., "Self-formed straight rivers with equilibrium banks and mobile bed, Part 1. The sand-silt river", Journal of Fluid Mechanics, London, England, Vol. 89, Part 1, pp. 109-126, 1978.
15- Pozovskii, I. L., "Flow of water in Bends of open channels", Academy of Sciences of U.S.S.R., Kiev, U.S.S.R, 1957.
16- Syunsuke, et al., "Bed topography in bends of sand-silt rivers", Journal of hydraulic Engineering, ASCE, Vol. 111, No. 11, November 1985.
17- Van Bendegom, L., "Eenige beschouwingen over riviermorphologie en rivierverbetering", De Ingenieur, Vol. 59, No. 4, pp. 1-11, 1947.
18- Yen, C., L., "Bed topography effect on flow in a meander", Journal of Hydraulics Division, ASCE, Vol. 96, No. HY1, pp. 57-73, 1974.
19- Zimmermann, C., and Kennedy, J. F., "Transverse bed slopes in curved alluvial streams", Journal of Hydraulics Division, ASCE, Vol. 104, No. HY1, pp. 33-48, 1978.

Appendix

Table (1) Different properties at the different bend locations.

Cross Sec. No.	Locat. (Km)	R_{out} (m)	R_{inn} (m)	R_{cent} (m)	A (m^2)	P (m)	$\bar{H}$ (m)	H (m)
1	91.550	529	462	495	256.2	106	3	4.2
2	92.200	354	266	300	307	119	4.5	5.5
3	96.850	548	380	500	309	169	2.3	2.7
4	101.400	528	385	480	309	155	2.8	3.7
5	102.800	942	798	900	412.1	178	4.5	7.4
6	104.150	1240	1134	1200	256	114	2.5	4.3
7	105.150	1038	921	1000	377	131.5	3.9	5.5
8	110.100	307.5	212	220	314	142	4.2	6.3
9	111.850	357	203	250	477	186	3.7	6
10	112.700	765	663	720	398	173	2.8	3.6
11	118.100	760	644	700	381.4	155	2.6	3.8
12	119.650	950	802	900	532	233	4.8	6.5
13	123.100	572	511	550	226	111	5	6.5
14	129.900	625	457	550	496	197	4.5	6.2
15	158.350	409	382	355	781	289	8	9.8
16	166.750	429	371	400	862	316	7.5	9.8
19	186.150	407	273	357	1004	344	5.6	7.8
20	194.100	1731	1194	1367	1088	364	5.6	7.8
17	170.050	527	473	500	916	335	8	10.5
18	172.800	2010	1596	1728	953	341	8.3	10.5
21	200.050	1102	827	1018	1205	357	11.4	13.5

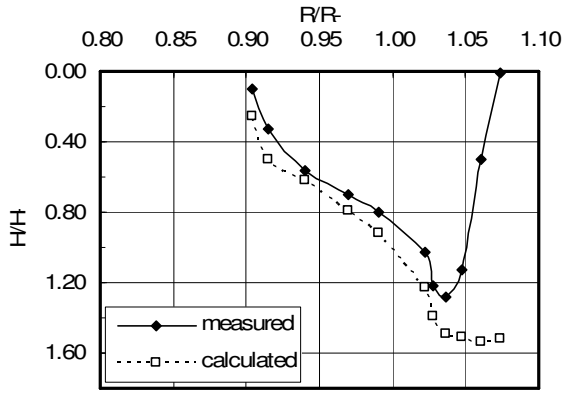

Fig. (1) Relationship between dimensionless flow depth and dimensionsless radius at km 91.550.

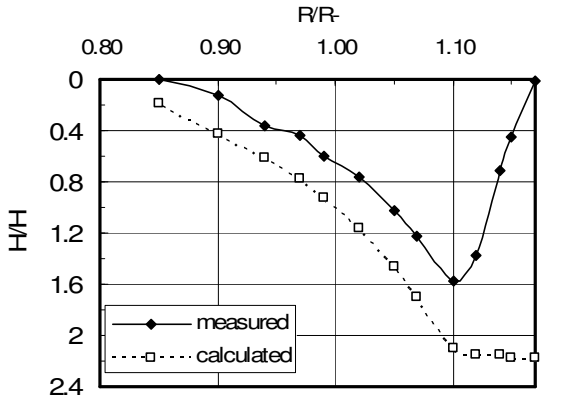

Fig. (2) Relationship between dimensionless flow depth and dimensionsless radius at km 92.250.

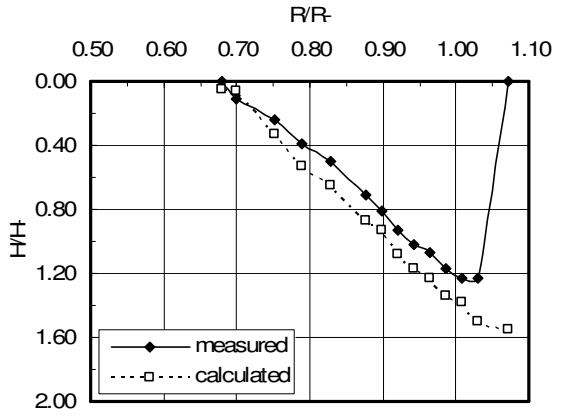

Fig. (3) Relationship between dimensionless flow depth and dimensionsless radius at km 101.550.

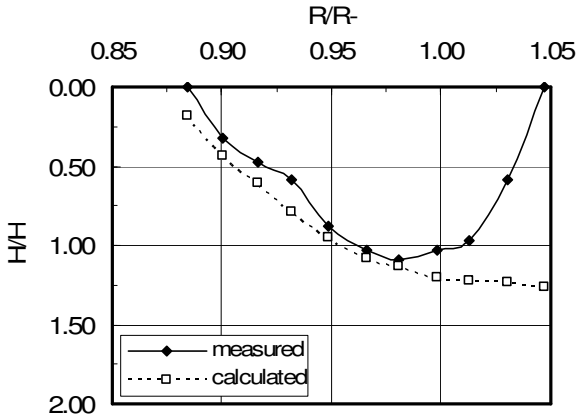

Fig. (4) Relationship between dimensionless flow depth and dimensionsless radius at km 103.00.

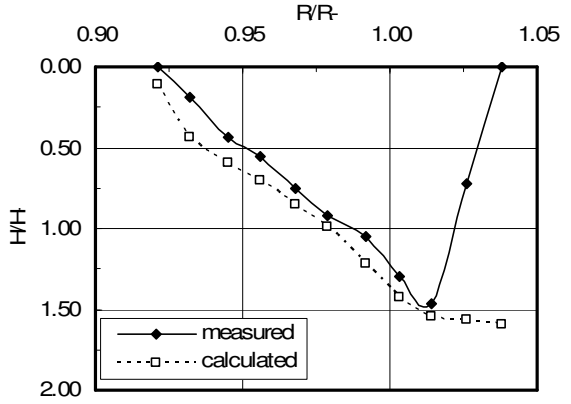

Fig. (5) Relationship between dimensionless flow depth and dimensionsless radius at km 105.150.

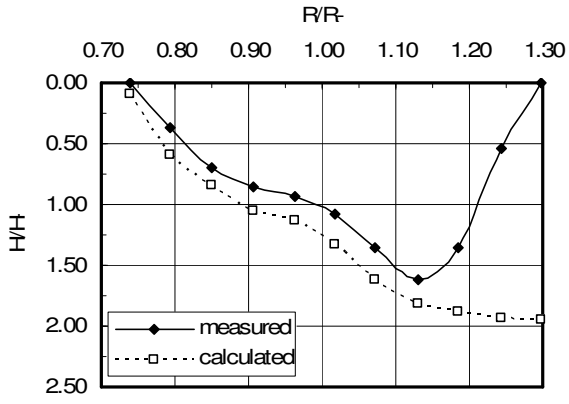

Fig. (6) Relationship between dimensionless flow depth and dimensionsless radius at km 113.650.

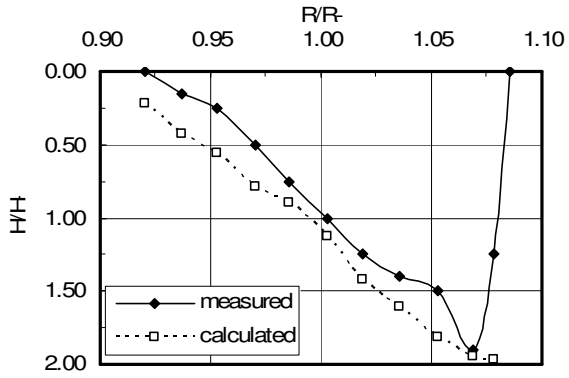

Fig. (7) Relationship between dimensionless flow depth and dimensionsless radius at km 118.100.

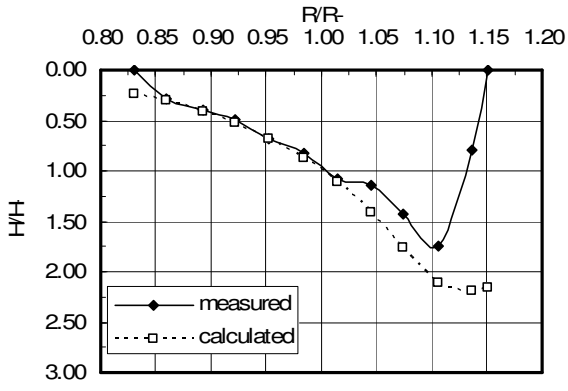

Fig. (8) Relationship between dimensionless flow depth and dimensionsless radius at km 129.900.

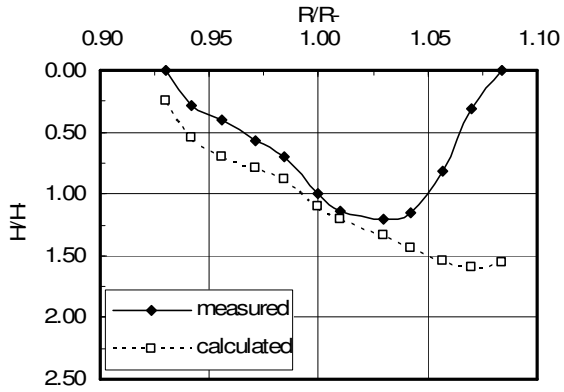

Fig. (9) Relationship between dimensionless flow depth and dimensionsless radius at km 158.350.

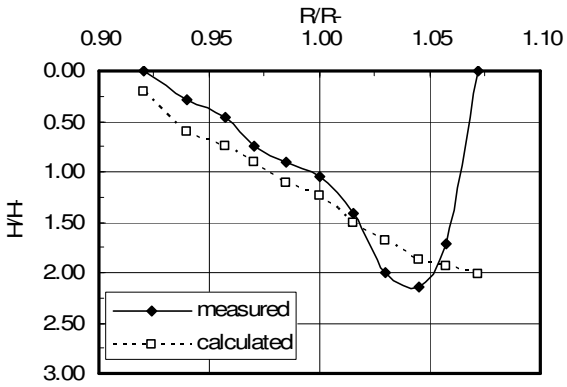

Fig. (10) Relationship between dimensionless flow depth and dimensionsless radius at km 166.750.

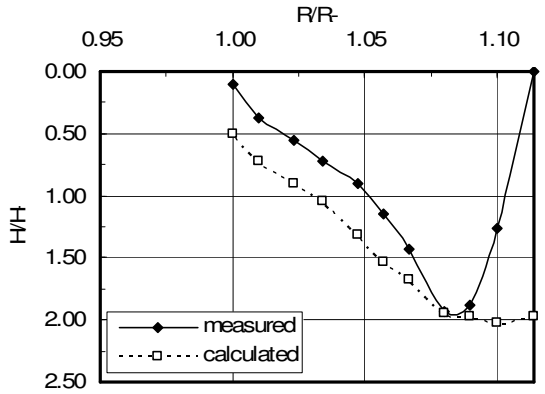

Fig. (11) Relationship between dimensionless flow depth and dimensionsless radius at km 170.050.

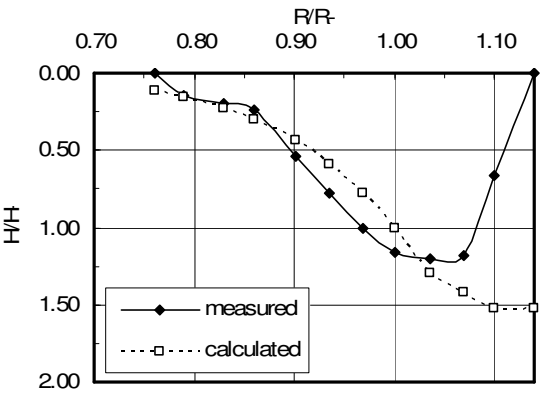

Fig. (12) Relationship between dimensionless flow depth and dimensionsless radius at km 186.150.

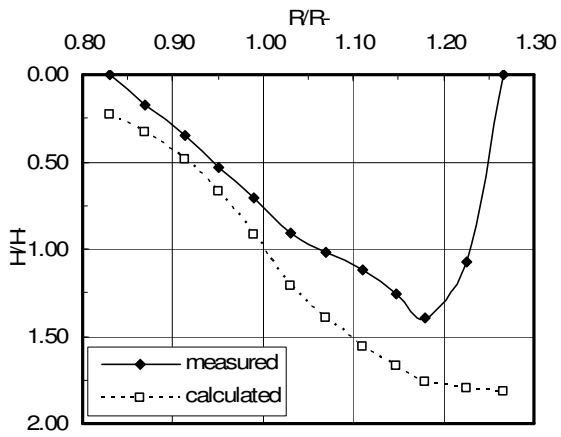

Fig. (13) Relationship between dimensionless flow depth and dimensionsless radius at km 194.100.

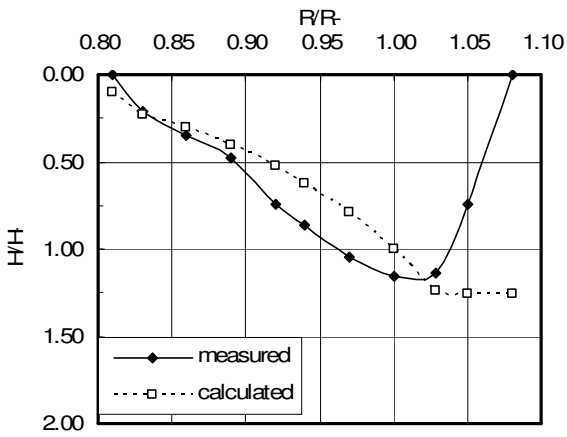

Fig. (14) Relationship between dimensionless flow depth and dimensionsless radius at km 200.50.

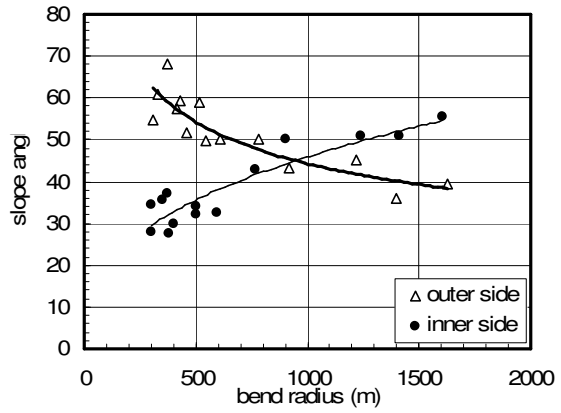

Fig. (15) Relationship between the outer bank slope angle and the outer radius.

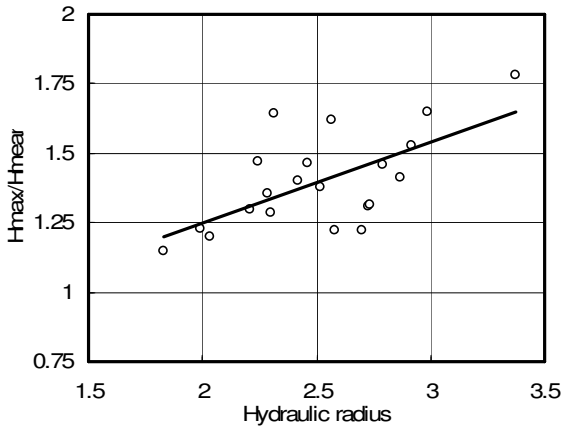

Fig. (16) Relationship between Hmax./Hmean and hydr. radius.